Int. J. Rock Mech. Min. Sci. & Geomech. Abstr. Vol. 28, No. 1, pp. 43–51, 1991
Printed in Great Britain.

0148-9062/91 $3.00 + 0.00

Identification of Nonlinear Fracture Properties From Size Effect Tests and Structural Analysis Based on Geometry-dependent *R*-curves

Z. P. BAŽANT†
R. GETTU†
M. T. KAZEMI†

The size effect method, previously developed for concrete and mortar, is demonstrated for rock. Geometrically similar fracture specimens of limestone are tested and the measured maximum load values are used to obtain fracture energy, fracture toughness and effective size of the fracture process zone. Further, it is shown how to determine, from these results, other nonlinear fracture parameters including the critical effective crack-tip opening displacement. R*-curves, dependent on specimen geometry, are calculated and used to predict load–deflection curves, which are found to agree very well with measurements. A modification of the* R*-curves for post-peak response is proposed.*

INTRODUCTION

Fracture mechanics has emerged as an important tool in the modelling of rock fragmentation, excavation by dynamic and hydraulic fracturing techniques, tunnelling and drilling [1]. Fracture properties have been taken into account in the studies of rock bursts [2], geothermal reservoirs [3, 4], formation of rock joints [5] and stability of rock slopes [6]. Whereas early studies have relied mainly on linear elastic fracture mechanics (LEFM), it is now generally recognized that the nonlinearity of fracture, caused by the existence of a sizable zone of microcracking and crack bridging near the crack tip (e.g. [7]), must be taken into account in the analysis of these problems.

In order to quantify the fracture properties of rock, several experimental techniques have been proposed. ISRM has proposed two chevron-notched core-based fracture specimens as standard methods for the determination of fracture toughness [1, 8]. Since rock cores are usually most convenient, many other researchers have also emphasized core-based tests (e.g. [9, 10]). An alternative method based on nonlinear fracture mechanics is proposed here which can be used to obtain various fracture parameters including the fracture toughness.

The most important consequence of fracture mechanics is the effect of structure or specimen size on failure load. For nonlinear fracture mechanics, the size effect is more complicated and represents a gradual transition between the size effects of LEFM and plasticity. This phenomenon has been well-documented in rock mechanics literature [11–16]. The objectives of this paper are to analyze this effect, and demonstrate the evaluation of nonlinear fracture properties from it. Another aim is to examine the applicability of the *R*-curve method for calculating structural response, and present a modified, experimentally justified version of this approach.

REVIEW OF SIZE EFFECT LAW

Size effect on failure loads may be defined by considering geometrically similar structures (or specimens) of different sizes and introducing the nominal stress at failure:

$$\sigma_N = c_n \frac{P_u}{bd}, \tag{1}$$

where P_u = maximum (ultimate) load, b = thickness, d = characteristic dimension of the structure or specimen and c_n = arbitrary coefficient introduced for convenience; its choice can be arbitrary since only relative values of σ_N matter for the analysis. One could set $c_n = 1$ (as in the calculations of the following section) to eliminate it. However, it might be preferable to set it equal to a convenient constant; e.g. for a Brazilian split-cylinder test, $c_n = 2/\pi$ would make σ_N equal to the maximum tensile stress based on elastic analysis.

†Center for Advanced Cement-Based Materials, Northwestern University, Evanston, IL 60208, U.S.A.

Plastic limit analysis, as well as elastic analysis with an allowable stress criterion, exhibits no size effect (i.e. geometrically similar structures of different sizes fail at the same σ_N). This is not, however, true for fracture mechanics. To illustrate this, we consider the total potential energy of a linear elastic structure $U = V(\sigma^2/2E')k(\alpha)$ where $V = v_0 bd^2 =$ volume of the structure (v_0 is some constant), $\sigma = P/bd =$ nominal stress, $P =$ load; $k(\alpha)$, which characterizes the shape of the structure, is a function of $\alpha = a/d$; $a =$ crack length, $E' = E$ for plane stress, $E' = E/(1-\nu^2)$ for plane strain, $E =$ Young's modulus for elasticity and $\nu =$ Poisson's ratio. Therefore, the energy release rate is $G = -(\partial U/\partial a)/b = -(\partial U/\partial\alpha)/bd = -v_0 d(\sigma^2/2E')k'(\alpha)$, from which:

$$G = \frac{P^2 g(\alpha)}{E' b^2 d}, \quad K_I = \sqrt{GE'} = \frac{Pf(\alpha)}{b\sqrt{d}}, \tag{2}$$

where $k'(\alpha) = dk(\alpha)/d\alpha$, $g(\alpha) = -k'(\alpha)\, v_0 c_n^2/2$ and $f(\alpha) = \sqrt{g(\alpha)}$. The values of $f(\alpha)$ are obtained according to LEFM [17].

When $g'(\alpha) > 0$, LEFM indicates that the maximum load occurs at infinitesimal crack extension. Then, $\alpha \simeq \alpha_0 = a_0/d$, where $a_0 =$ initial crack or notch length. When $P = P_u$, setting $G = G_f$ (fracture energy) or $K_I = K_{Ic}$ (fracture toughness or critical stress intensity factor), equation (2) results in $\sigma_N =$ constant$/\sqrt{d}$—the size effect of LEFM. Note that in this paper, only 2-D similarity is treated; for the case of 3-D similarity the reader is referred to [18].

In brittle-heterogeneous materials such as rock, concrete and ceramics, there is a fracture process zone of considerable size ahead of the continuous crack. This zone starts from zero size and grows as the load increases, while remaining attached to the notch tip. If the structure is not large, the process zone length is significant compared to a_0, in which case the equivalent crack length $a = a_0 + c$ at failure must be distinguished from a_0, where $c =$ elastically equivalent crack extension giving the same compliance according to LEFM as the actual crack growth. Then, G is the energy release rate for the elastically equivalent crack.

Let c_f denote the value of c in an infinitely large structure ($d \to \infty$) at maximum load, and G_f the corresponding value of G required for crack growth. For $d \to \infty$, we have $c/d \to 0$ and $\alpha \to \alpha_0$, which imply that in an infinitely large specimen, the fracture process zone occupies an infinitesimal volume fraction of the structure. Therefore, the structure as such can be treated as elastic. It follows that the stress and displacement fields surrounding the process zone must be the near-tip asymptotic elastic fields. These fields are independent of specimen geometry, and so the shape and size of the process zone should also be the same for any geometry.

Consequently, unambiguous definitions of G_f and c_f, independent of specimen shape, can be stated as follows [16, 18]: G_f and c_f are the energy required for crack growth and the elastically equivalent length of the fracture process zone, respectively, in an infinitely large specimen. Mathematically, for $d \to \infty$, $G_f = \lim G_m = \lim (K_{Im}^2/E')$, where G_m and K_{Im} are equal to G and K_I calculated from the measured peak load P_u and $\alpha = \alpha_0$ using equation (2). The fracture toughness can also be similarly defined.

The value of G required for crack growth depends on the process zone size. Since the value of c is essentially determined by this size, G for a growing crack may be assumed to be a function of c (which serves as the basis of the R-curve concept). The value of α at $P = P_u$, which depends on c (since $\alpha = \alpha_0 + c/d$), determines the value of $g(\alpha)$, and so the ratio $G/g(\alpha)$ at maximum load of a specimen of any size should be approximately equal to $G_f/g(\alpha_f)$ at infinite size, where $\alpha_f = \alpha_0 + c_f/d$. Therefore, $G \simeq G_f g(\alpha)/g(\alpha_f)$. Now we substitute this expression into equation (2), introduce the approximation $g(\alpha_f) \simeq g(\alpha_0) + g'(\alpha_0)\,(\alpha_f - \alpha_0)$ (based on Taylor series expansion), set $P_u^2 = (\sigma_N bd/c_n)^2$ [from equation (1)] and solve for σ_N [16]:

$$\sigma_N = c_n \left(\frac{E' G_f}{g'(\alpha_0) c_f + g(\alpha_0) d} \right)^{1/2}, \tag{3}$$

which is the size effect law, originally proposed in an equivalent general form [19]:

$$\sigma_N = \frac{B f_u}{\sqrt{1+\beta}}, \quad \beta = d/d_0. \tag{4}$$

Here B and d_0 are constants; and f_u is some arbitrary measure of material strength introduced for the sake of dimension (its value is immaterial since only the value of Bf_u matters).

Equation (3) may alternatively be put in a shape-independent form, as [16]:

$$\tau_N = \left(\frac{E' G_f}{c_f + \bar{d}} \right)^{1/2}, \tag{5}$$

where $\tau_N = \sqrt{g'(\alpha_0)}\; P_u/bd$, $\bar{d} = dg(\alpha_0)/g'(\alpha_0)$, $\tau_N =$ intrinsic nominal stress at failure and $\bar{d} =$ intrinsic (equivalent) size of the structure. The quantity that makes $\bar{d}$ shape-independent is the ratio $g(\alpha_0)/g'(\alpha_0)$ [16]. This ratio has also been used by other researchers in [20] and [21]. Variable τ_N is shape-independent because all the constants in equation (5) are material properties. Equations (3–5) are valid for both two and three dimensions.

Based on equations (3) and (4), G_f [22, 23], c_f [16] and K_{Ic} can be simply related to the size effect parameters as:

$$G_f = \frac{B^2 f_u^2}{c_n^2 E'} d_0 g(\alpha_0), \tag{6}$$

$$c_f = \frac{d_0 g(\alpha_0)}{g'(\alpha_0)}, \tag{7}$$

$$K_{Ic} = \sqrt{E' G_f} = \frac{B f_u}{c_n} \sqrt{d_0 g(\alpha_0)}. \tag{8}$$

The infinite size for which the above quantities have been defined must not be interpreted literally but needs to be regarded as a size about one order of magnitude beyond the range for which the size effect law has been calibrated [23].

For $\beta \gg 1$, equation (4) gives the approximation $\sigma_N \propto d^{-1/2}$ (for $\beta = 10$, the error is under 5%), which is the size effect exhibited by LEFM. For small values of β, equation (4) yields $\sigma_N = Bf_u$ = constant (for $\beta = 0.1$, again the error is under 5%), that is, there is no size effect. For $0.1 < \beta < 10$, the size effect is transitional between LEFM and plastic limit analysis (Fig. 1); in this range nonlinear fracture mechanics must be employed. Consequently, parameter β has been called the brittleness number, and is capable of characterizing the type of failure regardless of structure geometry [22, 23].

The size effect law has also been derived more generally on the basis of dimensional analysis and similitude arguments, and crack band analysis [18, 19].

The apparent fracture toughness K_{Im} can be determined by LEFM methods as if $\alpha = \alpha_0$ at failure. In that case, from equation (2), $K_{Im} = P_u\sqrt{g(\alpha_0)}/b\sqrt{d}$. Substituting $P_u = \sigma_N bd/c_n$ [equation (1)], and using $G_f = K_{Ic}^2/E'$ in equations (3–5), we obtain [22]:

$$K_{Im} = K_{Ic}\left(\frac{\bar{d}}{\bar{d}+c_f}\right)^{1/2} = K_{Ic}\left(\frac{\beta}{1+\beta}\right)^{1/2}. \qquad (9)$$

Equations (3–5) and (9) have the advantage that parameters B and d_0 or G_f and c_f (or K_{Ic} and c_f) can be determined from the measured peak loads P_u by linear regression [19] based on $Y = AX + C$, in which:

$$X = d, \quad Y = (f_u/\sigma_N)^2, \quad B = 1/\sqrt{C}, \quad d_0 = C/A. \qquad (10)$$

The size range of the specimens used in the regression must be sufficiently large in relation to the inevitable random scatter of material properties and test measurements. For the typical scatter of concrete the minimum size range is 1:4. This seems to be a reasonable range for rock as well.

Equation (4) has been shown to agree well with concrete fracture tests of different geometries [22] for Mode I as well as Mode II [24] and Mode III [25]. A good agreement was also demonstrated with some limited data for rock [16], certain ceramics [26] and aluminium alloys [27].

For specimen geometries for which $g'(\alpha)$ is initially negative and $g(\alpha)$ attains a minimum at $\alpha = \alpha_{min}$, P_u occurs according to LEFM when $\alpha = \alpha_0$ or α_{min}, whichever is smaller [28]. Tests with $g'(\alpha) < 0$ are stable even under load control and easier to control than the tests in which $g'(\alpha) > 0$. In such cases, equation (3) cannot be applied because $\alpha \to \alpha_{min}$ (as $d \to \infty$) for which $g'(\alpha) = 0$. However, equation (4) would still characterize the size effect, and equation (6) would yield G_f. Also, the value of Bf_u can be obtained from plastic analysis. So, even in cases where $g'(\alpha) < 0$, the size effect method can be used [29]. On the other hand, corrections can be applied (usually based on the stable crack growth before failure) or restrictions imposed on the specimen size to obtain the true material fracture toughness [1, 9, 15, 30, 31].

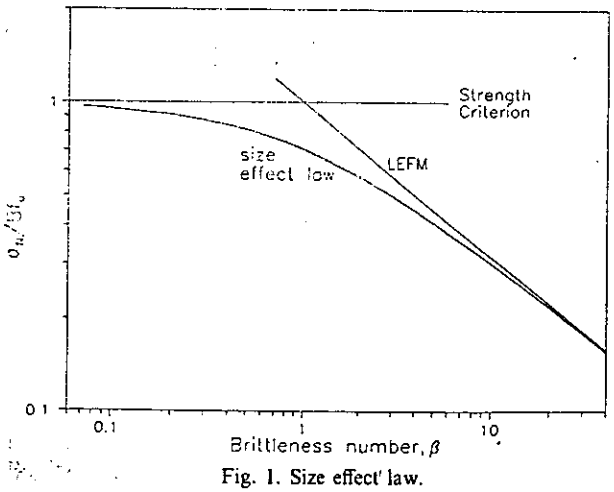

Fig. 1. Size effect law.

TESTS AND DETERMINATION OF FRACTURE PROPERTIES

This paper reports an experimental study of the size effect method for Indiana (Bedford) limestone, the fracture properties of which have been extensively tested [11, 30–32].

30-μm thick sections of the rock were used to determine the maximum grain size (Figs 2 and 3). Measurements were made through microscopy and computerized image analysis. The distinct grains were found to range from 0.1 to 1.5 mm (0.004 to 0.05 in) in size. Splitting tension tests were conducted on three cores, 54 mm (2.1 in) in diameter and 102 mm (4 in) in length. The average strength, 3.45 MPa (500 psi), was taken as the value of f_u. This gives an estimate of the strength of the limestone used. The mass density of the rock was 2.2 g/cm^3 (138 lb/ft^3).

Fracture tests were conducted on geometrically similar three-point (single edge-notched) bend specimens

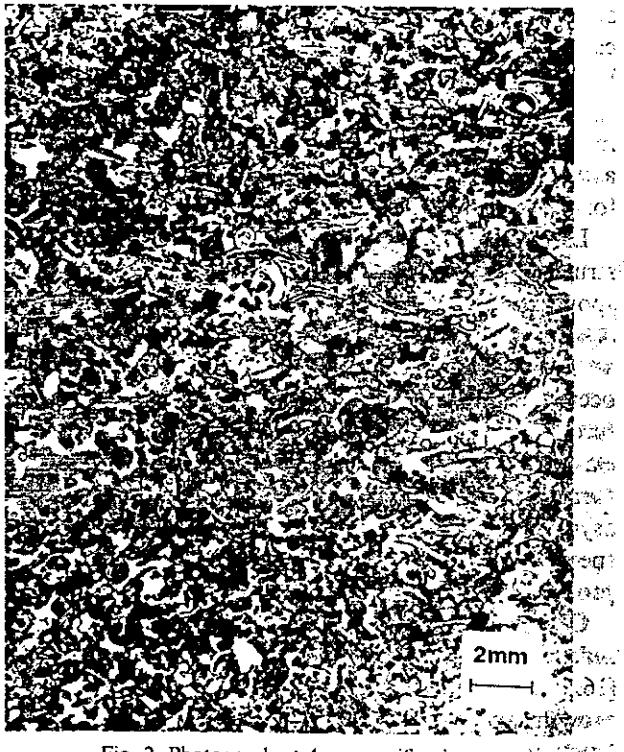

Fig. 2. Photograph at 4× magnification.

Fig. 3. Photograph at 30× magnification.

(Fig. 4) of depths $d = 102, 51, 25, 13$ mm (4, 2, 1, 0.5 in) and of the same thickness 13 mm (0.5 in). The notches were 1.3 mm (0.05 in) wide. Specimens were cut from a single block of rock, with their notches normal to the natural bedding plane (known as the arrester orientation). The specimens were supported on aluminium bearing plates of 1.6 mm (0.063 in) thickness and length $d/2$, which were glued to the rock with epoxy. It should be noted that, despite the anisotropy of Indiana limestone, the effect of crack orientation on fracture toughness has been reported as negligible [11].

The beams were tested in a closed-loop controlled 90 kN (20 kip) MTS testing frame with a load cell operating in the 0.89 kN (200 lb) range. The measured crack mouth opening displacement (CMOD) was used as feedback to run the tests at constant CMOD rate. CMOD control was essential for stable crack propagation beyond the peak load. Loading rates were such that peak loads were reached in about 8 min. Load-line displacements were measured between the cross-head of the loading ram and the tension face of the specimen. The test setup is shown in Figs 5 and 6. Typical load–displacement and load–CMOD curves are shown in Figs 7 and 8 (the displacements of the smallest specimens were not determined since the gauge was larger than the available space between the supports). The peak loads obtained are given in Table 1.

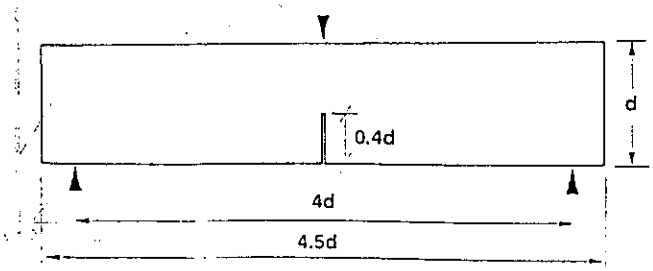

Fig. 4. Specimen geometry tested.

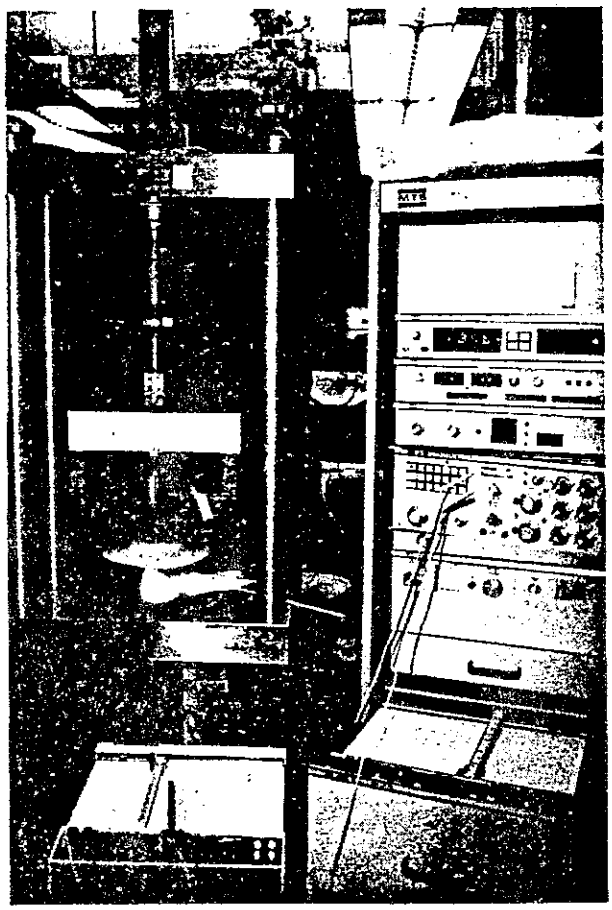

Fig. 5. Complete setup for closed-loop testing.

The modulus of elasticity was obtained for each beam by equating the initial load–CMOD compliance to the theoretical elastic value; the average was $E = 15.3$ GPa (2.2×10^6 psi), with coefficient of variation = 25%. Poisson's ratio ν was assumed as 0.15.

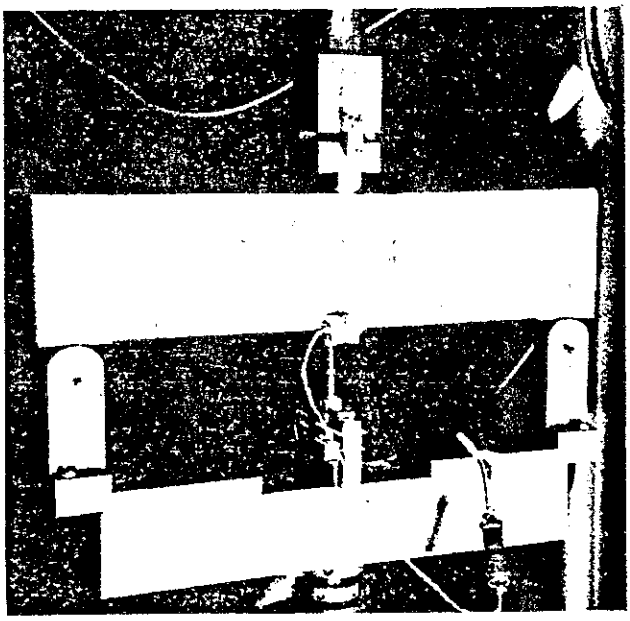

Fig. 6. Specimen test configuration.

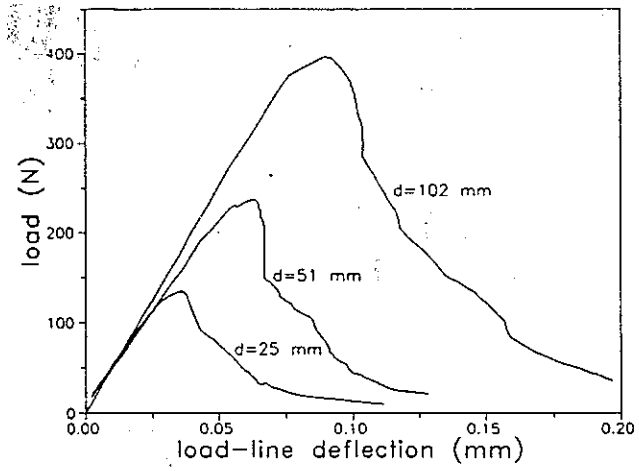

Fig. 7. Typical load–deflection curves.

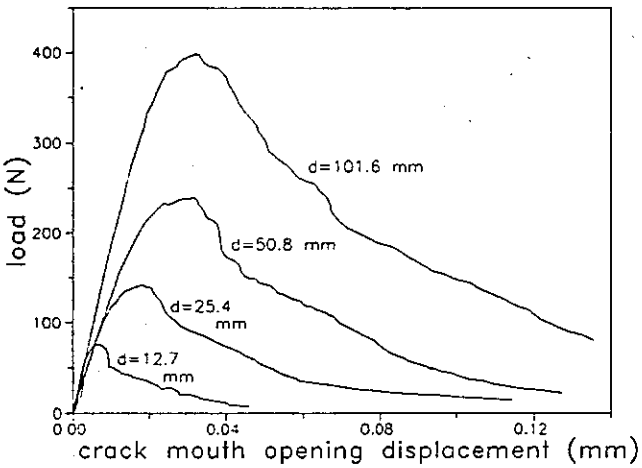

Fig. 8. Typical load–CMOD curves.

In the analysis, factor c_n was taken as 1 for convenience. The linear regression plot using equation (10), shown in Fig. 9, gives $A = 0.80\ \text{mm}^{-1}$ (20.3 per in), with standard error = 6% and $C = 41.3$, with standard error = 7%. The coefficient of variation of the deviations of Y from the regression line is 7%. From equation (10), the size effect parameters are $B = 0.156$ and $d_0 = 51.6$ mm (2.03 in).

Figure 10 shows the size effect curve based on the calculated parameters. Note that all the data points lie in the transition zone between the LEFM criterion and the strength criterion. This shows that evaluation of

Table 1

Specimen dimensions (mm × mm × mm)	Peak load (N)
457 × 102 × 13	418
	405
	394
229 × 51 × 13	238
	243
	243
114 × 25 × 13	134
	140
	140
57 × 13 × 13	82
	85
	78

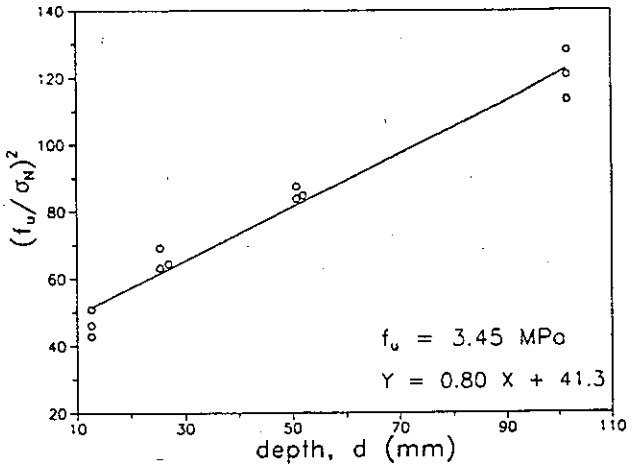

Fig. 9. Regression line for size effect parameters.

these specimens by LEFM cannot yield size-independent values of the fracture parameters. From the measured size effect curve it appears that, for the specimen geometry considered here, the beam depth would have to exceed 1300 mm (51 in) for LEFM [equation (2) with $P = P_u$ and $\alpha = \alpha_0$] to be applicable (error less than 2%).

The fracture toughness K_{Ic} has been evaluated from equation (8), assuming the specimens to be in plane stress ($E' = E$). Using $g(\alpha_0) = 62.84$ (from [17]), we obtain $K_{Ic} = 0.969\ \text{MPa}\sqrt{\text{m}}$ (881 psi$\sqrt{\text{in}}$); coefficient of variation = 3%. This value is in good agreement with the results of other studies on Indiana limestone. Schmidt [11] tested three-point bending fracture specimens of different sizes (almost the same as in the present study) and used LEFM relations but with effective crack lengths determined from compliance calibrations, to obtain the fracture toughness for each specimen. The values were found to approach 0.99 MPa$\sqrt{\text{m}}$ (900 psi$\sqrt{\text{in}}$) for the largest specimens. From short-rod fracture tests, Barker [31] obtained values for the fracture toughness, modified by a so-called "plasticity" correction procedure to eliminate size-dependence, the average of which was 1.13 MPa$\sqrt{\text{m}}$ (1028 psi$\sqrt{\text{in}}$). An average fracture toughness value of 1.05 MPa$\sqrt{\text{m}}$ (954 psi$\sqrt{\text{in}}$) was reported by Ingraffea *et al.* [30], also from short-rod tests.

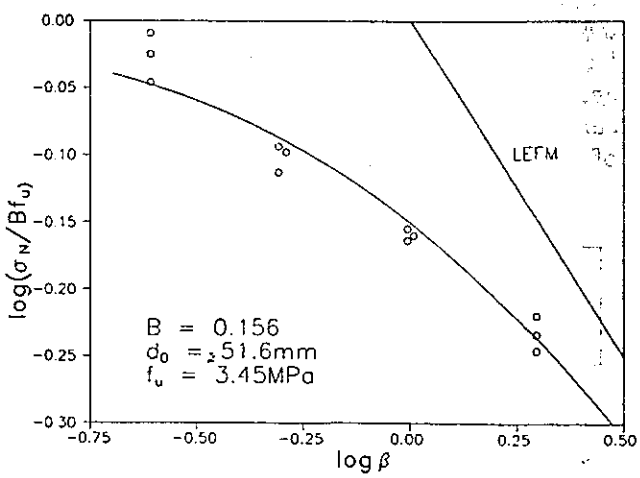

Fig. 10. Plot of size effect curve.

The dependence of the apparent fracture toughness K_{Im} on the specimen size is plotted in Fig. 11 along with the predicted trend given by equation (9).

The fracture energy of the limestone can be evaluated from equation (6). Substituting the average value of E, we obtain $G_f = 61$ N/m (0.35 lb/in). The other fracture parameter, the elastically equivalent process zone length, results from equation (7) using $g(\alpha_0) = 62.84$, $g'(\alpha_0) = 347.7$ (from [17]); $c_f = 9.3$ mm (0.37 in); coefficient of variation = 9%.

It has been suggested that the fracture energy of brittle heterogeneous materials can be determined from the area W_0 under the measured load–deflection diagram of a fracture specimen. In this method [33, 34], the total energy dissipated during the test is taken as $W = W_0 + mg\ u_f$ where mg = weight of specimen and u_f = final deflection when the beam breaks. The fracture energy is obtained as $G_w = W/(d - a_0)b$, and the corresponding fracture toughness is $K_{Iw} = \sqrt{E'G_w}$. From Fig. 12 it is clear that G_w increases with beam depth and that the specimen size should be considerably large for the G_w-value to be size-independent. Similarly, the K_{Iw} values are also size-dependent.

RELATION TO SOME OTHER FRACTURE PROPERTIES

Other nonlinear fracture characteristics can be deduced from size effect tests by using LEFM relations. By extrapolation to infinite size, these characteristics become shape and size independent. For example, the crack surface displacements behind the tip are, according to LEFM [17], $v = -(K_I/\mu)\ (r/2\pi)^{1/2} \sin\phi(2 - 2\bar{\nu} + \cos^2\phi)$ where $\phi = \vartheta/2$, r and ϑ = polar co-ordinates centred at the crack tip, K_I = Mode I stress inensity factor, $\bar{\nu} = \nu/(1+\nu)$ for plane stress, $\bar{\nu} = \nu$ for plane strain and $\mu = E/2(1+\nu)$. For an infinitely large specimen, the equivalent elastic crack-tip opening displacement δ_{CTOD} at the peak load can be obtained by substituting $r = c_f$ and $K_I = K_{Ic}$:

$$\delta_{CTOD} = v|_{\vartheta=\pi} - v|_{\vartheta=-\pi} = \frac{8K_{Ic}}{E'}\sqrt{\frac{c_f}{2\pi}}. \qquad (11)$$

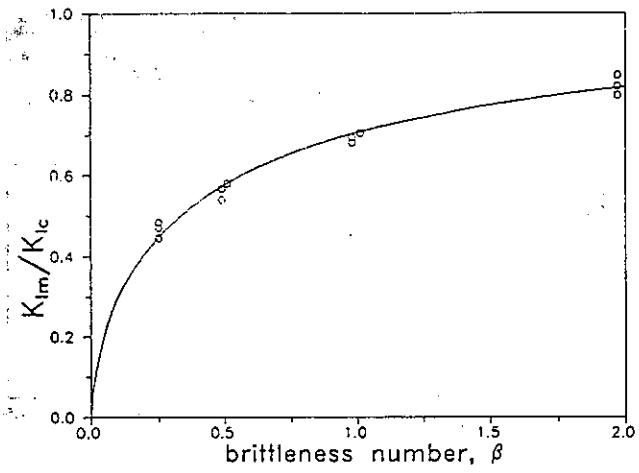

Fig. 11. Variation of apparent fracture toughness with size.

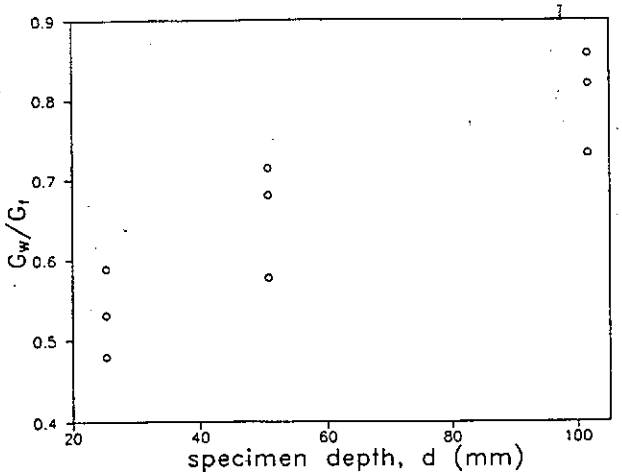

Fig. 12. Variation of fracture energy based on work fracture.

From the present test results, $\delta_{CTOD} = 0.019$ mm (0.75×10^{-3} in).

Jenq and Shah [35] estimated material tensile strength from fracture mechanics by considering a large double-edge notched specimen in tension with a very small crack [for which $g(\alpha_0) \to 0$]. A similar exercise with the size effect law [equation (3)], based on $\alpha_0 = 0$, $g(0) = 0$ and $g'(0) = 3.955$ [35], yields $f_t = 0.503\, K_{Ic}/\sqrt{c_f}$. For the Indiana limestone tested, this gives $f_t = 5.0$ MPa (730 psi), while the measured splitting tensile strength was 3.45 MPa. The difference in values may partially be attributed to the effects of size and geometry.

In computational nonlinear fracture models such as the crack band model [36] and the fictitious crack model [37], the softening relation in the fracture process zone is defined in terms of G_f and f_0, the local or microscopic tensile strength. Note that f_0 is not quite interchangeable with the values determined from experiments which are macroscopic averaged size-dependent quantities. In the fictitious crack model, the behaviour of the fracture process zone is characterized by a relation of stress f to the opening δ of an equivalent (fictitious) crack, and in the crack band model by a relation of stress f to average strain $\bar{\varepsilon} = \delta/w_c$ of an equivalent crack band of width w_c. The fracture energy is $G_f = \int f(\delta)\, d\delta$, where $f(\delta \geq \delta_f) = 0$ and $f(0) = f_0$.

As an example, consider $f(\delta)$ to be a linear relation, $f = f_0\,(1 - \delta/\delta_f)$ (a popular assumption due its simplicity), in which case $G_f = f_0\delta_f/2$. For this, Planas and Elices [21] obtained $f_0 = 0.65\, K_{Ic}/\sqrt{c_f}$. Substituting the values calculated earlier, $f_0 = 6.5$ MPa (940 psi). The value of f_0 is higher than f_t (strength from size effect parameters obtained from tests) and f_t (from the splitting tests mentioned earlier), which give the tensile strength of a test specimen with a very small notch. From the calculated value of f_0, we can obtain $\delta_f = 2G_f/f_0 = 0.019$ mm (0.75×10^{-3} in). This value is practically the same as δ_{CTOD} computed from equation (11).

To sum up, if G_f and c_f are determined from size effect tests, other nonlinear fracture parameters such as the critical effective crack-tip opening displacement and the local tensile strength can be easily deduced.

PREDICTION OF STRUCTURAL RESPONSE FROM R-CURVES

The size of the fracture process zone evolves as it propagates. Consequently, the resistance $R(c)$ to fracture growth, representing energy dissipated per unit length of crack extension, varies. Function $R(c)$, called the R-curve [38, 39], used to be considered a material property, approximately independent of the shape of the specimen or structure. It has, however, been shown that R-curves, for certain materials, depend strongly on the specimen geometry (e.g. [40]). Ref. [40] demonstrates that the size effect law can be used to obtain R-curves.

It is possible to calculate the structural response by identifying the size effect law, determining from it the R-curve, and finally using it along with LEFM relations. The R-curve corresponding to the size effect law is given by the expression [16]:

$$R(c) = G_f \frac{g'(\alpha)}{g'(\alpha_0)} \frac{c}{c_f}, \tag{12}$$

in which

$$\frac{c}{c_f} = \frac{g'(\alpha_0)}{g(\alpha_0)} \left(\frac{g(\alpha)}{g'(\alpha)} - \alpha + \alpha_0 \right). \tag{13}$$

These equations define the R-curve parametrically. Note that here α is merely a dummy parameter. After determining G_f and c_f, a series of α-values may be chosen and for each of them the length c of an elastically equivalent crack (free of bridging stresses) calculated from equation (13), and then $R(c)$ determined from equation (12).

For readers' convenience, the derivation of equations (12) and (13) is briefly presented as follows. The energy balance at failure requires that $F(c, d) = G(\alpha, d) - R(c) = 0$. If we increase the size slightly from d to $d + \delta d$ but retain the geometry (i.e. $\alpha_0 = \text{constant}$), failure now occurs at $c + \delta c$, and since $G = R$ must also hold for $c + \delta c$, we must have $\partial F/\partial d = 0$. Mathematically, the condition $\partial F/\partial d = 0$ together with $F(c, d) = 0$ means that the R-curve is the envelope of a family of fracture equilibrium curves $F(c, d) = 0$ for various values of d [40]. Because the R-curve is size-independent, $\partial R/\partial d = 0$ and so $\partial G/\partial d = 0$. Now we may substitute $P_u^2 = (\sigma_N bd/c_n)^2 = (Bf_u bd/c_n)^2/(1 + d/d_0)$ where $(Bf_u)^2 = c_n^2 E' G_f/d_0 g(\alpha_0)$ [according to equation (6)] into $G = P_u^2 g(\alpha)/E' b^2 d$ [i.e. equation (2)]. We thus obtain for the critical states:

$$G(\alpha, d) = G_f \frac{g(\alpha)}{g(\alpha_0)} \frac{d}{d + d_0}. \tag{14}$$

Substituting this into $\partial G/\partial d = 0$, differentiating and noting that $\partial\alpha/\partial d = \partial\alpha_0/\partial d + \partial(c/d)/\partial d = -c/d^2 = -(\alpha - \alpha_0)/d$ (because $\partial\alpha_0/\partial d = 0$ for geometrically similar structures), we get:

$$\frac{d + d_0}{d_0} = \frac{g(\alpha)}{(\alpha - \alpha_0) g'(\alpha)}. \tag{15}$$

Furthermore, substituting this along with the relations $(\alpha - \alpha_0)\, d = c$ and $d_0 = c_f g'(\alpha_0)/g(\alpha_0)$ [from equation (7)] into equation (14), and setting $G(\alpha, d) = R(c)$, equation (13) is proven. Also, elimination of d from equation (15) yields equation (12).

In the foregoing derivations, no simplifications other than those for the size effect law were made. The objective was to maintain a one-to-one relation between the R-curve and size effect law so that both would predict the same failure loads. If one were to simplify the R-curve of equation (12) by taking $g'(\alpha) \simeq g'(\alpha_0)$, a linear relation for the pre-peak regime, $R(c) = G_f\, c/c_f$, results. However, this form would correspond to a complex and geometry-dependent size effect law that would be very different from equation (3). The determination of fracture parameters and the modelling of the peak loads of different-size specimens would then become more complicated. Therefore, the R-curve of equation (12) is preferred. Also, it has been shown experimentally that a linear R-curve is insufficient for modelling the nonlinear fracture process in rock [41]. As shown later, the present R-curve predicts the nonlinear response of the specimens satisfactorily.

The derivation of equations (12) and (13) presumed that the fracture process zone remains attached to the tip of the initial crack or notch. We now assume that the fracture process zone gets detached from the tip and advances ahead with approximately constant size and dissipates roughly the same amount of energy per unit crack extension. Consequently, G after peak load should be constant and equal to the value that $R(c)$ has reached at the peak load. These assumptions will be verified by comparing predictions based on them to experimental data. The model based on these assumptions is, of course, simplified (Fig. 13)—in reality the deviation from the R-curve probably comes about gradually and smoothly.

Based on fracture tests, investigators have reported that R-curves are dependent on the size and geometry of the specimen as well as the notch length [27, 35, 42, 43]. Our preceding calculation of the R-curve indicates that this phenomenon has principally two sources: (1) the effect of $g'(\alpha)$ and $g(\alpha)$ which depend on specimen geometry [16]; and (2) the deviation of G from the R-curve after the peak load, as already explained. Other minor effects, however, may also contribute to the

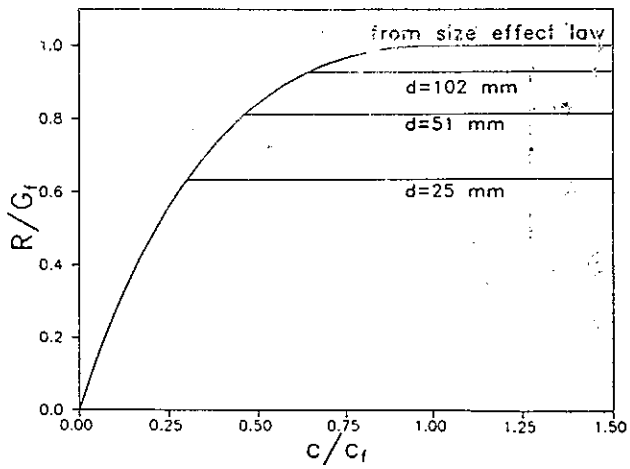

Fig. 13. Effect R-curves.

dependence of R-curves on size and geometry. As concluded from tests on ceramic specimens [43], interaction of the fracture process zone and the specimen boundary can even lead to falling R-curve behaviour after a plateau is exhibited. However, the declining part of the R-curve is significant only for specimens with very small uncracked ligaments and usually affects only the final part of the post-peak response.

Let u_c = load-line displacement due to fracture alone, u_0 = displacement calculated as if there were no crack, and $u = u_c + u_0$ = total displacement. To calculate u_c, we proceed as follows. We first determine W_P, the total energy released if the fracture occurred at constant load P. Since $\partial W_P/\partial a = bG = P^2 g(\alpha)/E'bd$, we have $W_P = b\int G(a)\,da = P^2 \int g(\alpha)\,d\alpha/E'b$. According to Castigliano's second theorem:

$$u_c = \frac{\partial W_P}{\partial P} = \frac{2P}{E'b}\int_0^\alpha g(\alpha')\,d\alpha'. \tag{16}$$

At the same time, for $G = R$:

$$P = b\sqrt{\frac{E'd}{g(\alpha)}\,R(c)} = \frac{b\sqrt{d}}{f(\alpha)}\,K_{IR}(c), \tag{17}$$

where $K_{IR}(c)$ is the effective fracture resistance corresponding to the R-curve, defined as $K_{IR}(c) = \sqrt{E'R(c)}$. Choosing various values of α, u_c and P can be calculated for each of them. Thus, equations (16) and (17) define the load–deflection curve parametrically.

To calculate the total displacement, the elastic deflections u_b and u_s due to bending and shear in the specimen without any crack must be added to u_c. Assuming plane stress conditions, $u_0 = u_b + u_s$, $u_b = PL^3/4Ebd^3$ (bending), $u_s = 0.6\,(1+\nu)\,PL/Ebd$ (shear). The weight of the beam is approximately taken into account by modifying P and u as $P_t = P - (mg/2)$, $u_t = u - u_w$, where mg = weight of the specimen and u_w = initial deflection due to self-weight (estimated from the initial compliance and weight of the specimen).

Figure 14 compares the predictions obtained with the present R-curve method to the measured load–deflection curves for three different sizes. The predictions agree with the test results quite well. If a rising R-curve is used for the post-peak response, the calculated deflections grossly disagree with tests. This confirms the validity of the aforementioned model for the R-curve and its post-peak modification.

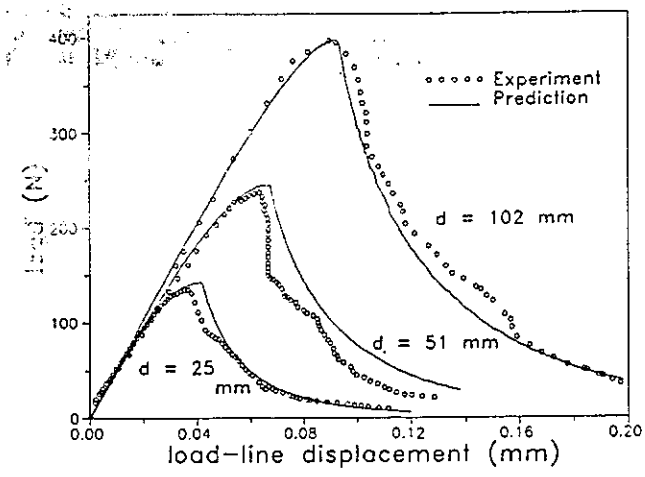

Fig. 14. Prediction of structural response.

CONCLUSIONS

1. The size effect method is based on the fact that extrapolation to an infinitely large specimen can be used for unambiguous and shape-independent definition of fracture energy (or fracture toughness) and the effective length of the fracture process zone. With this method, nonlinear material fracture properties can be determined solely from the measured maximum loads of geometrically similar specimens of sufficiently different sizes. The applicability of this method, which has previously been demonstrated for concrete, mortar and granite, is now verified for limestone. Based on these studies, this method seems applicable to rock in general.
2. Since the size effect law is uniquely related to the R-curve for a given specimen geometry, the latter can also be determined solely from the measured maximum loads. The R-curve so obtained can be used only for calculating the specimen response up to the maximum load. Under the assumption that the energy required for crack growth remains constant after the peak load, the predicted post-peak deflections agrees well with measurements on rock.

Acknowledgements—The underlying study of the size effect law was partially supported under AFOSR Contract F 49620-87-C-0030DEF with Northwestern University, and this paper was written under partial support from the Center for Advanced Cement-Based Materials at Northwestern University (NSF Grant DMR-8808432) and from a cooperative project with Universidad Politecnica de Madrid funded under U.S.–Spain Treaty Grant CCA-8309071. The authors are grateful to M. R. Tabbara for developing the software used for modelling the structural response.

Accepted for publication 9 September 1990.

REFERENCES

1. International Society for Rock Mechanics Commission on Testing Methods. Suggested methods for determining the fracture toughness of rock (Co-ordinator Ouchterlony F.). *Int. J. Rock Mech. Min. Sci. & Geomech. Abstr.* 25, 71–96 (1988).
2. Fairhurst C. and Cornet F. H. Rock fracture and fragmentation. *Rock Mechanics from Research to Applications, 22nd U.S. Symp. Rock Mech.*, Massachussetts Institute of Technology (1981).
3. Bažant Z. P., Ohtsubo H. and Aoh K. Stability and post-critical growth of a system of cooling and shrinkage cracks. *Int. J. Fract.* **15**, 443–456 (1979).
4. Takahashi H. Application of rock fracture mechanics to HDR geothermal reservoir design. Preprints of the *Proc. Int. Workshop on Fracture Toughness and Fracture Energy—Test Methods for Concrete and Rock*, Sendai, Japan, pp. 453–472 (1988).
5. Kemeny J. and Cook N. G. W. Formation and stability of steeply dipping joint sets. *Research & Engineering Applications in Rock Masses, 26th U.S. Symp. Rock Mech.* Balkema, Boston (1985).
6. Tharp T. M. and Coffin D. T. Field application of fracture mechanics analysis to small rock slopes. *ibid.*
7. Labuz J. F., Shah S. P. and Dowding C. H. Experimental analysis of crack propagation in granite. *Int. J. Rock Mech. Min. Sci. & Geomech. Abstr.* **22**, 85–98 (1985).

8. Ouchterlony F. On the background to the formulae and accuracy of rock fracture toughness measurements using ISRM standard core specimens. *Int. J. Rock Mech. Min. Sci. & Geomech. Abstr.* **26**, 13–23 (1989).
9. Karfakis M. D., Chong K. P. and Kuruppu M. D. A critical review of fracture toughness testing of rocks. *Rock Mechanics: Key to Energy Production, 27th U.S. Symp. Rock Mech.*, Soc. of Min. Engnrs (1986).
10. Chong K. P., Li V. C. and Einstein H. H. Size effects, process zone and tension softening behavior in fracture of geomaterials. *Engng Fract. Mech.* **34**, 669–678 (1989).
11. Schmidt R. A. Fracture-toughness testing of limestone. *Expl Mech.* May, 161–167 (1976).
12. Schmidt R. A. and Lutz T. J. K_{Ic} and J_{Ic} of Westerly granite—effects of thickness and in-plane dimensions. *Fracture Mechanics Applied to Brittle Materials*, ASTM STP 678, pp. 166–182 (1979).
13. Weisinger R., Costin L. S. and Lutz T. J. K_{Ic} and J-resistance-curve measurements on Nevada tuff. *Expl Mech.* **20**, 68–72 (1980).
14. Costin L. S. Static and dynamic fracture behavior of oil shale. *Fracture Mechanics Methods for Ceramics, Rocks and Concrete*, ASTM STP 745, pp. 169–184 (1981).
15. Matsuki K. Size effect and size requirement in fracture toughness evaluation of rock. Preprints of the *Proc. Int. Workshop of Fracture Toughness and Fracture Energy—Test Methods for Concrete and Rock*, Sendai, Japan (1988).
16. Bažant Z. P. and Kazemi M. T. Determination of fracture energy, process zone length and brittleness number from size effect, with application to rock and concrete. *Int. J. Fract.* **44**, 111–131 (1990).
17. Tada H., Paris P. C. and Irwin G. R. *The Stress Analysis of Cracks Handbook*, 2nd Edn. Paris Productions, St Louis (1985).
18. Bažant Z. P. Fracture energy of heterogeneous materials and similitude. Preprints, *SEM/RILEM Int. Conf. on Fracture of Concrete and Rock* (Houston) (Shah S. P. and Swartz S. E., Eds), pp. 170–177. Soc. for Exp. Mech. (1987); also in *Fracture of Concrete and Rock SEM-RILEM Int. Conf.* (Shah S. P. and Swartz S. E., Eds), pp. 229–241. Springer-Verlag, New York (1989).
19. Bažant Z. P. Size effect in blunt fracture: concrete, rock, metal. *J. Engng Mech. Div. ASCE* **110**, 518–535 (1984).
20. Horii H., Hasegawa A. and Nishino F. Fracture process and bridging zone model and influencing factors in fracture of concrete. *Fracture of Concrete and Rock SEM-RILEM Int. Conf.* (June 1987, Houston) (Shah S. P. and Swartz S. E., Eds) pp. 205–219. Springer-Verlag, New York (1989).
21. Planas J. and Elices M. Size-effect in concrete structures: mathematical approximations and experimental validation. Preprints, *France–U.S. Workshop, Strain Localization and Size Effect due to Cracking and Damage* (Paris) (Mazars J. and Bažant Z. P., Eds) (1988).
22. Bažant Z. P. and Pfeiffer P. A. Determination of fracture energy from size effect and brittleness number. *ACI Mater. J.* **84**, 463–480 (1987).
23. Bažant Z. P. Fracture in concrete and reinforced concrete. Preprints, *IUTAM Prager Symp. on Mechanics of Geomaterials: Rocks, Concretes, Soils* (Evanston) (Bažant Z. P., Ed.) (1983); also in *Mechanics of Geomaterials, Rocks, Concrete, Soils* (Bažant Z. P., Ed.), pp. 259–304. Wiley, Chichester (1985).
24. Bažant Z. P. and Pfeiffer P. A. Shear fracture tests of concrete. *Mater. Struct. (RILEM, Paris)* **19**, 111–121 (1986).
25. Bažant Z. P. and Prat P. C. Measurement of Mode III fracture energy of concrete. *Nucl. Engng Des.* **106**, 1–8 (1988).
26. Bažant Z. P. and Kazemi M. T. Size effect in fracture of ceramics and its use to determine fracture energy and effective process zone length. *J. Am. Ceram. Soc.* **73**, 1841–1853 (1990).
27. Bažant Z. P., Lee S.-G. and Pfeiffer P. A. Size effect tests and fracture characteristics of aluminum. *Engng Fract. Mech.* **26**, 45–57 (1987).
28. Shannon J. L. Jr and Munz D. G. Specimen size and geometry effects on fracture toughness of aluminum oxide measured with short-rod and short-bar chevron-notched specimens. *Chevron-Notched Specimens: Testing and Stress Analysis*, ASTM STP 855 (Underwood J. H., Freiman S. W. and Baratta F. I., Eds), pp. 152–166 (1983).
29. Marti P. Size effect in double-punch tests on concrete cylinders. *ACI Mater. J.* **86**, 597–601 (1989).
30. Ingraffea A. R., Gunsallus K. L., Beech J. F. and Nelson P. P. A short-rod based system for fracture toughness testing of rock. *Chevron-Notched Specimens: Testing and Stress Analysis*, ASTM STP 855 (Underwood J. H., Freiman S. W. and Baratta F. I., Eds), pp. 152–166 (1983).
31. Barker L. M. K_{Ic} measurements using short rod specimens—the elastic plastic case. Terra Tek Report 77-91R, Salt Lake City (1977).
32. Ingraffea A. R. Fracture propagation in rock. *Mechanics of Geomaterials, Rocks, Concrete, Soils* (Bažant Z. P., Ed.), pp. 219–258. Wiley, Chichester (1985).
33. Tattersall H. G. and Tappin G. The work of fracture and its measurement in metals, ceramics and other materials. *J. Mater. Sci.* **1**, 296–301 (1966).
34. Hillerborg A. The theoretical basis of a method to determine the fracture energy G_F of concrete. *Mater. Struct. (RILEM, Paris)* **18**, 291–296 (1985).
35. Jenq Y. S. and Shah S. P. A two parameter fracture model for concrete. *J. Engng Mech. Div. ASCE* **111**, 1227–1241 (1985).
36. Bažant Z. P. and Oh B. H. Rock fracture via strain-softening finite elements. *J. Engng Mech. Div. ASCE* **110**, 1015–1035 (1984).
37. Hillerborg A., Modeer M. and Petersson P. E. Analysis of crack formation and crack growth in concrete by means of fracture mechanics and finite elements. *Cem. Concr. Res.* **6**, 773–782 (1976).
38. ASTM Special Committee on Fracture Testing of High-Strength Sheet Materials. Report. *ASTM Bull.* Jan, 29–40 (1960).
39. Krafft J. M., Sullivan A. M. and Boyle R. W. Effect of dimensions on fast fracture instability of notched sheets. *Crack Propagation Symp., Proc.*, Cranfield, U.K. (1961).
40. Bažant Z. P., Kim J.-K. and Pfeiffer P. A. Nonlinear fracture properties from size effect tests. *J. Struct. Div. ASCE* **112**, 289–307 (1986).
41. Ouchterlony F. A simple R-curve approach to fracture toughness testing of rock core specimens. *Issues in Rock Mechanics* (Goodman R. E. and Heuze F. E., Eds), pp. 515–522. Soc. of Min. Engnrs, New York (1982).
42. Adams N. J. Influence of configuration on R-curve shape and G_c when plane stress conditions prevail, *Crack and Fracture*, ASTM STP 601, pp. 330–345 (1976).
43. Sakai M., Yoshimura J.-I., Goto Y. and Inagaki M. R-curve behavior of a polycrystalline graphite: microcracking and grain bridging in the Wake region. *J. Am. Ceram. Soc.* **71**, 609–616 (1988).